Lattice parameters and Raman-active phonon modes of $(In_xGa_{1-x})_2O_3$ for $x < 0.4$

Christian Kranert, Jörg Lenzner, Marcus Jenderka, Michael Lorenz, Holger von Wenckstern, Rüdiger Schmidt-Grund, and Marius Grundmann

Citation: Journal of Applied Physics **116**, 013505 (2014); doi: 10.1063/1.4886895
View online: https://doi.org/10.1063/1.4886895
View Table of Contents: http://aip.scitation.org/toc/jap/116/1
Published by the American Institute of Physics

Lattice parameters and Raman-active phonon modes of $(In_xGa_{1-x})_2O_3$ for $x < 0.4$

Christian Kranert,[a] Jörg Lenzner, Marcus Jenderka, Michael Lorenz, Holger von Wenckstern, Rüdiger Schmidt-Grund, and Marius Grundmann
Institut für Experimentelle Physik II, Halbleiterphysik, Universität Leipzig, Linnéstr. 5, 04103 Leipzig, Germany

(Received 19 May 2014; accepted 23 June 2014; published online 3 July 2014)

We present X-ray diffraction and Raman spectroscopy investigations of $(In_xGa_{1-x})_2O_3$ thin films and bulk-like ceramics in dependence of their composition. The thin films grown by pulsed laser deposition have a continuous lateral composition spread allowing the determination of phonon mode properties and lattice parameters with high sensitivity to the composition from a single 2-in. wafer. In the regime of low indium concentration, the phonon energies depend linearly on the composition and show a good agreement between both sample types. We determined the slopes of these dependencies for eight different Raman modes. While the lattice parameters of the ceramics follow Vegard's rule, deviations are observed for the thin films. Further, we found indications of the high-pressure phase $InGaO_3$ II in the thin films above a critical indium concentration, its value depending on the type of substrate. © *2014 AIP Publishing LLC*. [http://dx.doi.org/10.1063/1.4886895]

I. INTRODUCTION

The large band gap of gallium oxide Ga_2O_3 of approximately 5 eV motivates its use in applications like high-power devices and ultraviolet (UV) photodetectors. Such photodetectors based on binary Ga_2O_3 are solar-blind, i.e., they are not sensitive to the terrestrial solar irradiation and therefore able to detect even weak artificial UV light sources during daylight. However, there is a gap between the edge of the solar spectrum and the cut-off energy of detectors based on binary Ga_2O_3. Alloying with In_2O_3 lowers the band gap such that $(In_xGa_{1-x})_2O_3$ -based photodetectors covering the complete solar-blind spectrum are feasible.

Fabrication of such devices requires the knowledge of basic properties of the active material. Particularly, for the $(In_xGa_{1-x})_2O_3$ compound, structural changes throughout the composition range are inevitable owing to the different crystal structures of monoclinic β-Ga_2O_3 and bixbyite-type bcc-In_2O_3. This was previously investigated for powder samples prepared under equilibrium conditions by means of X-ray diffraction (XRD). For temperatures below 1400 °C and ambient pressures, no intermediate phase between β-Ga_2O_3 and bcc-In_2O_3 was observed, but only a mixture of these two phases within the miscibility gap for an In-content between 45 at. % and 95 at. %.[1,2] For preparation temperatures equal to or above 1550 °C, a different phase with an indium to gallium ratio of 1:1 was obtained.[3–5] Another phase of this stoichiometry was observed for samples prepared at a pressure of 65 kbar.[6]

Additionally to XRD, Raman scattering spectroscopy is well suited for the investigation of such structural changes due to its sensitivity to symmetry properties. Further, in case of a solid solution without secondary phases, the variation of the phonon energy with the composition can be used to determine the composition from the Raman spectra. Besides several publications on Raman scattering in binary β-Ga_2O_3 (single crystals[7] and powder samples[8]) and binary In_2O_3 (single crystals[9] and thin films[10]), only one report on the phonon modes in $(In_xGa_{1-x})_2O_3$ has been published,[5] where powder samples were investigated. Samples with only a few different indium concentrations were probed in this study showing a rather strong scattering in the respective data points. Hence a more accurate and denser data set and data for thin films are desirable. Further, the dependency on composition was only shown for three of the 15 Raman active phonon modes of the β-Ga_2O_3 structure.

Here, we present a combined XRD and Raman scattering study on 2-in. diameter $(In_xGa_{1-x})_2O_3$ thin films with a continuous composition spread (CCS) in comparison to bulk-like ceramic samples. From the measurements of the ceramic samples, we obtain the lattice parameters as a function of the composition in compliance with Vegard's rule. We further derived the phonon energy dependencies on the composition with a high precision from the Raman measurements. The CCS approach for the films allows us to determine their properties for virtually any composition within the composition range of the sample, also filling the gaps in the data for the ceramic samples. From the comparison of XRD and Raman results, we deduce possible causes for some features in the data for the thin films differing from the ceramic samples, e.g., the occurrence of an intermediate phase in the thin films for indium concentrations above a critical value.

II. EXPERIMENTAL SETUP AND SAMPLES

The $(In_xGa_{1-x})_2O_3$ thin film samples studied here were grown by means of pulsed laser deposition (PLD) using a segmented PLD source target and exhibit a continuous composition spread. For further details on the applied CCS technique, please refer to von Wenckstern *et al.*[11] We prepared the samples on 2-in. wafers of two different substrate materials: (00.1)-oriented α-Al_2O_3 (referred to as *c*-sapphire in the following) and (100)-oriented MgO. These substrate

[a]Electronic mail: christian.kranert@uni-leipzig.de

materials were chosen because the growth of Ga_2O_3 on them is well investigated and features an epitaxial relation between substrate and film. The β-Ga_2O_3 films grow with $(\bar{2}01)$ orientation on *c*-sapphire substrates and with (100) orientation on (100)-MgO substrate.[12–14] Oxygen pressures in the PLD chamber of 3×10^{-4} mbar for *c*-sapphire substrates and of 0.08 mbar for MgO substrates were chosen to obtain uniformly oriented films. The use of higher pressures for deposition on *c*-sapphire results in the additional formation of other orientations of the β-phase.[15] The other PLD parameters were identical for both substrate types: The substrate was heated to approximately 650 °C and the targets were ablated using a KrF excimer laser ($\lambda = 248$ nm) with a pulse energy of 600 mJ and a repetition rate of 15 Hz. Here, we discuss two films (A and B) grown on *c*-sapphire, which only differ in the total pulse count (75 000 and 150 000 pulses) and thereby in thickness, and one film grown on MgO (60 000 pulses). The resulting thicknesses are around 150 nm and 300 nm for the films on *c*-sapphire and 500 nm for the film on MgO. Thus, regarding the lattice mismatch,[12–14] the films are assumed fully relaxed.

Binary Ga_2O_3 and In_2O_3 films for comparison were grown on smaller (10×10 mm^2) substrates. We further compared our results to ceramic samples similar to the targets used for the PLD process. These were prepared by homogenization and pressing of Ga_2O_3 (5N purity) and In_2O_3 (4N5 purity) powders. Subsequently, they were sintered at 1350 °C for 72 h to assure a complete reaction between the two source materials.

Raman scattering was excited by means of a HeCd laser emitting at $\lambda_{exc} = 325$ nm. The light was focused and collected by a 50× microscope objective (backscattering geometry) with a numerical aperture of 0.40 yielding a lateral resolution of approximately 2 μm. Within this spot size, the composition gradient of the CCS samples is negligibly small. The collected light was analyzed for its linear polarization using a Glan-Thompson prism. The spectra were recorded by a Jobin Yvon U1000 double spectrometer equipped with two gratings with 2400 lines/mm. We used a liquid nitrogen cooled charge coupled device with 2048×512 square pixels with an edge length of 13.5 μm for detection. The spectral resolution was set to approximately 1 cm^{-1} at $\lambda_{exc} = 325$ nm.

The thin film composition was determined by means of energy dispersive X-Ray analysis (EDX) from the intensities of the K-lines of gallium and the L-lines of indium. Diffraction patterns of the ceramic samples were measured using a Philips X'pert diffractometer with Cu Kα radiation and Bragg-Brentano goniometer. Laterally, resolved X-Ray diffraction patterns were recorded using a PANalytical X'pert MRD pro diffractometer with Cu Kα radiation and a PIXcel^{3D} detector in 1D scanning mode with 255 channels. A programmable divergence slit yields an illuminated area of 1.5×10 mm. For the line scans, a step size of 1 mm was chosen.

III. RESULTS

A. EDX

The lateral variation of the composition of the thin films is shown in Fig. 1. For the thin film on MgO (100), we find

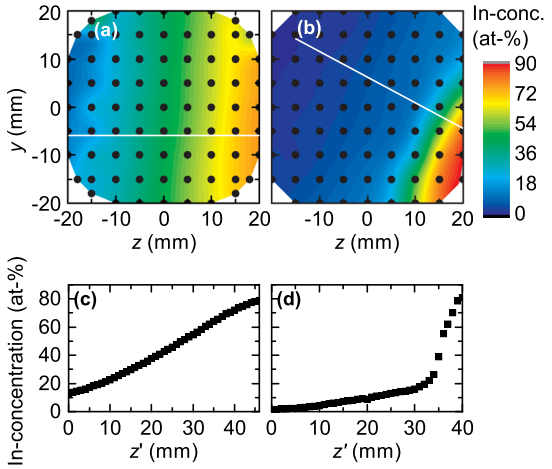

FIG. 1. Indium concentration of the CCS samples as determined by EDX measurements. Concentration mappings of films on (a) MgO (100) and (b) *c*-sapphire (sample A). The black circles mark the spots, where the concentration was actually measured. The false colour image results from an interpolation between these points. Position (0, 0) is situated at the center of the 2-in. wafer. (c) and (d) Line scans of the same samples along the white lines in (a) and (b).

that the variation of the In-content along the gradient has a slight S-shape inline with prediction from simulations of the CCS PLD process.[11] For the thin film on *c*-sapphire, a different behaviour is observed. For low In-content (below about 20 at. %), an almost linear increase of the In-concentration with the position z' is observed. For higher In-content ($z' \gtrsim 33$ mm), it increases rapidly. We discuss this observation below. The minimum indium concentration obtained for the film on MgO of approximately 10 at. % is much higher than for the film on *c*-sapphire, which has a minimum indium concentration below the detection limit of 0.5 at. %. This is probably caused by the higher oxygen pressure during growth for the MgO substrate, increasing the scattering especially of the lighter gallium atoms.

B. XRD

We measured powder diffraction patterns of our ceramic samples with different indium concentrations to determine their lattice parameters in dependence on the composition. No indications of In_2O_3 were found implying a full incorporation of the provided indium into the β-Ga_2O_3 lattice. We obtained the lattice parameters of the monoclinic unit cell by means of Rietveld refinement[16] using the PANalytical HighScore Plus 3.0.5 software and the values for binary β-Ga_2O_3 (Ref. 17) as initial structure. The resulting values are $a = (12.295 + 1.43x)$ Å, $b = (3.035 + 0.35x)$ Å, $c = (5.795 + 0.39x)$ Å, and $\beta = (103.9 - 3.3x)$ Å. These are compared to such reported in the literature[1,18] in Fig. 2. A good agreement is found, particularly with the data from bulk powder samples.[1]

The structural properties of the thin films were investigated by laterally resolved XRD. These data are shown in Figs. 3 and 4 for the samples grown on *c*-sapphire and MgO, respectively. Note that the plot for the sample on MgO is shown in dependence on the composition, while it is shown in dependence on the lateral position for the sample on *c*-sapphire, owing to its inhomogeneous composition gradient.

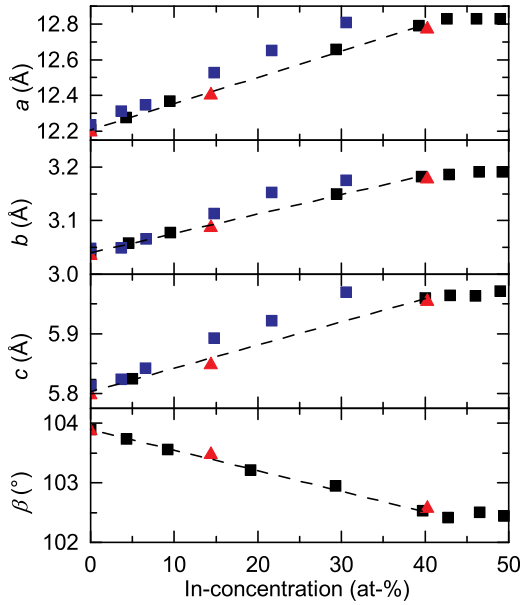

FIG. 2. Lattice parameters for $(In_xGa_{1-x})_2O_3$ samples in dependence on the indium concentration. Data from the literature for bulk powder[1] (black squares) as well as for thin film samples[18] (blue squares) are shown together with our own data from ceramic samples (red triangles). The dashed lines are guides to the eye.

Three regions can be distinguished: In the gallium-rich regime (bottom part of the false colour images), only peaks related to the β-type structure are observed, which are labelled as "G." This phase is $(\bar{2}01)$-oriented for growth on *c*-sapphire and (100)-oriented for growth on MgO, in agreement with other publications.[12–14] For the indium-rich regime, we observe peaks related to (111)-oriented bcc-In_2O_3, labelled as "I," for both samples. For the *c*-sapphire substrate, this is in agreement to the literature[19,20] and to binary In_2O_3 reference samples grown by us. For growth on MgO, both preferentially (100) (Ref. 21)- as well as (111)-oriented films[22] have been reported. We also observe both preferential orientations in our reference samples, depending on the deposition parameters. The intermediate region differs between the two substrates used: For *c*-sapphire, additional peaks labelled as "IG" at 28.8° and 59.8° occur already in the gallium-rich regime and become weaker with increasing indium concentration, but can still be observed for the indium-rich side of the sample. These peaks can be assigned to the (004) and (008) planes of the high-pressure phase $InGaO_3$ II.[6] For MgO, no XRD signal from the film could be detected within a large intermediate area $(0.4 \leq x < 0.65)$. However, we still observe the same additional peaks in the indium-rich regime.

In the gallium-rich regime, the peaks related to the β-Ga_2O_3 structure shift towards lower angles with increasing indium concentration for both samples. The dependence of the lattice plane distances on the composition obtained from this shift is depicted in Fig. 5. The *a* lattice parameter appears to be reduced with regard to the ceramic samples for the film grown on MgO (Fig. 5(a)), while the spacing of the $(\bar{2}01)$ planes is slightly increased for the film grown on *c*-sapphire (Fig. 5(b)). For indium concentrations up to approximately 20 at. %, the observed distances show a linear behaviour with a slope comparable to that obtained from the ceramic samples. For higher concentrations, the slope is significantly reduced for both substrates.

C. Raman spectroscopy

The β-modification of Ga_2O_3 has a monoclinic symmetry, which belongs to the space group $C2/m$. Its 27 optical phonon modes belong to the irreducible representation[7]

$$\Gamma^{opt} = 10A_g + 5B_g + 4A_u + 8B_u. \quad (1)$$

Phonon modes with A_g and B_g symmetries are Raman active, those with A_u and B_u symmetries are infrared active.

Raman spectra of the ceramic samples are shown in Fig. 6. For all concentrations, the observed Raman peaks match those of the β-Ga_2O_3 structure. They are labelled similarly to the publication of Vigreux *et al.*[5] for comparability. Peaks at spectral positions of two different phonon modes, which could not be resolved, are denoted with both indices. As in the XRD measurements, we did not find any hint on In_2O_3 in the samples. All modes show a clear redshift with increasing indium concentration as it is expected for the incorporation of the heavier and larger indium atoms into gallium oxide and also already observed by Vigreux *et al.*[5] We have extracted the composition dependences of seven Raman peaks by approximation with a linear function. These are summarized in Table I. Note that one of these peaks $(\omega_0 = 475\,cm^{-1})$ results from scattering by two phonon

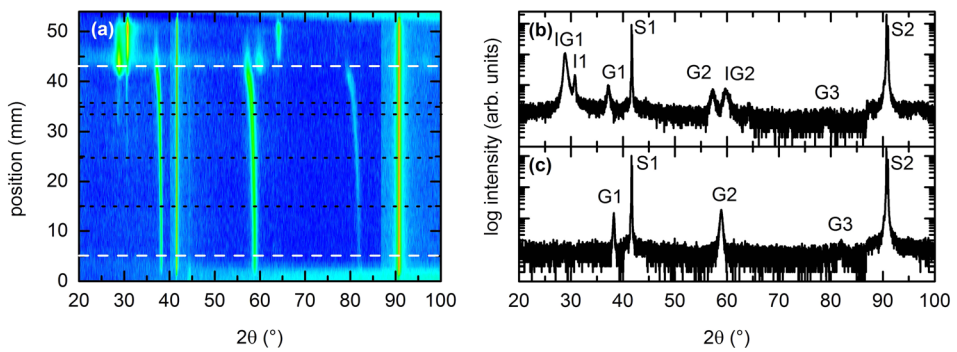

FIG. 3. (a) False colour plot of an XRD line scan of an $(In_xGa_{1-x})_2O_3$ CCS thin film on *c*-sapphire. The gallium-rich area corresponds to small position values. The dotted black lines indicate the positions, where the concentration equals to 5, 10, 15, and 20 at. %, respectively (from bottom to top). (b) and (c) Single 2θ-ω scans at the positions marked by white dashed lines in (a). The peaks are labelled as follows: S1/S2: Al_2O_3 (0002)/(0004), G1/G2/G3: β-Ga_2O_3 $(\bar{4}02)/(\bar{6}03)/(\bar{8}04)$, I1: bcc-$In_2O_3$ (222), IG1/IG2: $InGaO_3$ II (004)/(008).

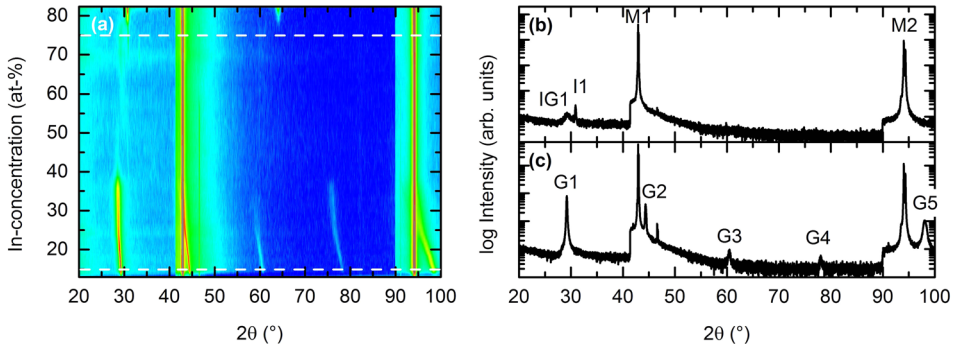

FIG. 4. (a) False colour plot of an XRD line scan of an $(In_xGa_{1-x})_2O_3$ CCS thin film on MgO (100). The *y*-scale has been converted from position to indium concentration based on the EDX results. (b) and (c) Single 2θ-ω scans at the positions marked by white dashed lines in (a). The steps at $2\theta \approx 41^\circ$ and 90° are due to the used Ni-filters, which cut the short wavelength bremsstrahlung below the absorption edge of Ni. The peaks are labelled as follows: M1/M2: MgO (200)/(400), G1/G2/G3/G4/G5: β-Ga_2O_3 (400)/(600)/(800)/(10 00)/(12 00), I1: bcc-In_2O_3 (222), IG1: $InGaO_3$ II (004).

modes with A_g and B_g symmetries, respectively, which cannot be discriminated in powder spectra.

For a comparison to the results obtained by Vigreux *et al.*,[5] we extracted the data points from Fig. 2 of that publication. We, then, carried out a linear approximation to these data analogously to the treatment of our own results. The range for this was limited to the range before the formation of secondary phases, specifically to $0 < x < 0.4$. These results are also summarized in Table I. The error in the data of Vigreux *et al.* is larger than what we obtain from our measurements and the slopes obtained by us are smaller, but they agree with each other within the error range.

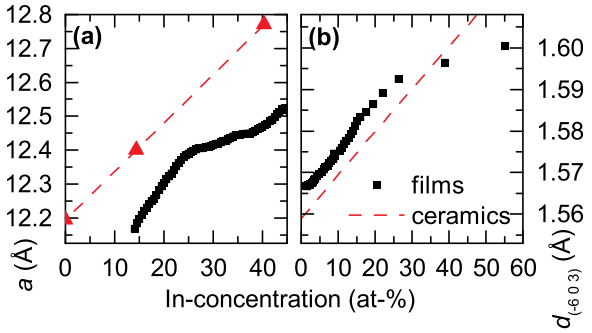

FIG. 5. Lattice plane distances determined from 2θ-ω-scans of $(In_xGa_{1-x})_2O_3$ CCS thin films grown on (a) MgO and (b) *c*-sapphire compared to data obtained for the ceramic samples. Red triangles in (a) represent the obtained lattice parameter *a* of the ceramic samples, the red dashed line is a guide to the eye. In (b), the red dashed line represents the spacing of the $(\bar{6}03)$ planes calculated from Vegard's rule for the lattice parameters obtained from the ceramic samples.

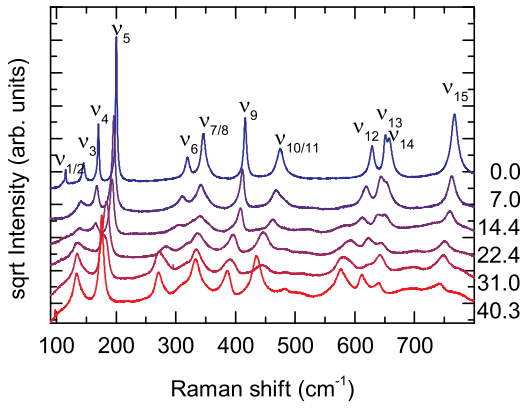

FIG. 6. Raman spectra of $(In_xGa_{1-x})_2O_3$ ceramic samples with the indium concentration given right to the graph in at. %, all excited at $\lambda_{exc} = 325$ nm. Peaks are labelled in accordance to Vigreux *et al.*[5]

Spectra for a CCS film grown on *c*-sapphire are shown in Fig. 7 for $0 < x < 0.12$ by means of a false colour image, together with spectra at the respective composition ends. A monotonic, linear shift of the Ga_2O_3 phonon modes can be observed without the splitting of any modes, as indicated by the dashed lines. Also no additional peaks appear. This implies that the phonons of this alloy show one-mode behaviour and that no secondary phase could be detected in this composition range.

For films on *c*-sapphire, some of the phonon modes of the thin film are superimposed by the strong Raman lines from the substrate. This is not the case for Raman inactive MgO substrates. Raman spectra of films grown on MgO are shown in Fig. 8. We observe a monotonic and mainly linear redshift for several phonon modes marked by straight dashed lines in the figure. The spectral positions of these peaks in dependence on the composition are shown in Fig. 9 (red squares) together with the data for the films grown on *c*-sapphire (blue and green squares) and for the ceramic samples (red triangles). Note that data for the samples grown on *c*-sapphire are missing in Fig. 9(b). This peak cannot be observed for these samples due to the strong A_{1g} mode of *c*-sapphire at 417 cm^{-1}.

TABLE I. Slopes of the energy shift with In-concentration *x* for several phonon modes of $(In_xGa_{1-x})_2O_3$. All values given in cm^{-1}, errors are the doubled standard deviations of the linear approximation.

			$\frac{d\omega}{dx}$	
Mode	ω_0 (cm^{-1})	Symmetry	This work	Vigreux *et al.*[5]
ν_5	200	A_g	-64 ± 5	-75 ± 11
ν_6	319	A_g	-125 ± 17	n/a
ν_9	416	A_g	-79 ± 5	-92 ± 13
$\nu_{10/11}$	475	A_g/B_g	-101 ± 9	n/a
ν_{12}	629	A_g	-131 ± 13	n/a
ν_{13}	651	B_g	-98 ± 9	n/a
ν_{14}	658	A_g	-45 ± 8	n/a
ν_{15}	767	A_g	-66 ± 4	-80 ± 17

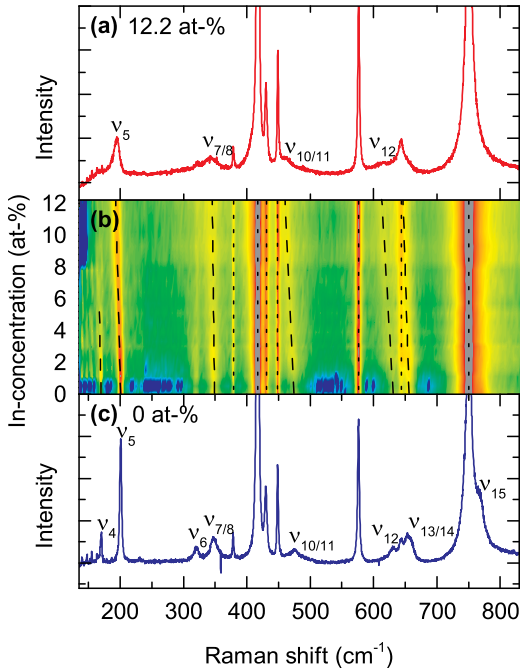

FIG. 7. Raman spectra of an $(In_xGa_{1-x})_2O_3$ CCS thin film sample grown on *c*-sapphire. (b) False colour image based on Raman spectra of an $(In_xGa_{1-x})_2O_3$ CCS thin film sample grown on *c*-sapphire measured at 18 positions with different indium concentrations. The straight dashed lines indicate peaks from the thin film and the vertical dotted lines such from the substrate, both are guides to the eye. (a) and (c) show the spectra from the points of highest and lowest indium concentrations of (b), respectively.

For indium concentrations higher than 20 at. % in the films grown on *c*-sapphire, we observe changes in the spectra compared to data for lower *x*, most strikingly the raise of a peak at 260 cm^{-1} (see Fig. 10). It cannot be assigned to any

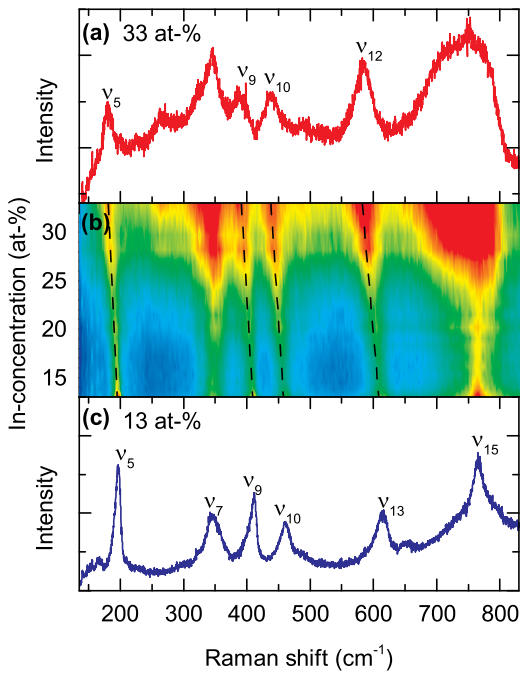

FIG. 8. (b) False colour image based on Raman spectra of an $(In_xGa_{1-x})_2O_3$ CCS thin film sample grown on MgO measured at 18 positions with different indium concentrations. Dashed lines are guides to the eye. (a) and (c) show the spectra from the points of highest and lowest indium concentrations of (b), respectively.

of the phonon modes of the β-Ga_2O_3 structure as well as to that of bcc-In_2O_3.[10] Thus, this indicates the presence of an intermediate phase in our PLD-grown films, probably $InGaO_3$ II, as already observed by XRD (see Figs. 3 and 4). The peak also appears for the film grown on MgO substrate, but much weaker and only for indium concentrations above approximately 30 at. % (see Fig. 8(a)).

IV. DISCUSSION

The lattice parameters of our ceramic samples show a good agreement to Vegard's rule and the values reported in the literature.[1] Thus, we can assume that our bulk samples are single-phase and the indium is fully incorporated into the β-Ga_2O_3 host lattice. This is substantiated by the obtained dependencies of the phonon mode energies on the composition, which show a mainly linear behaviour. Our Raman data exhibit a considerably lower scatter and, thus, higher accuracy as compared to the data published by Vigreux *et al.*[5] This difference is probably related to the error in the determination of the composition. To verify this, we used the slopes obtained by us and the data points for the ν_5 peak at $\omega_0 = 200\,cm^{-1}$ of Vigreux *et al.* to recalculate the indium concentrations in their powders. Indeed, if we, then, plot the other two phonon energies, for which data points were presented in this publication, in dependence on the recalculated composition, we obtain much smoother, linear curves with slopes very close to the values obtained by us $((-80 \pm 4)\ cm^{-1}$ for ν_9 and $(-72 \pm 6)\ cm^{-1}$ for $\nu_{15})$.

For the CCS thin film samples, the deviation of the lattice plane spacings from the bulk values might be related to the growth conditions. Indeed, for growth of films without composition spread on identical substrates, we observe a decreasing out-of-plane lattice spacing with increasing oxygen pressure during growth (cf. Lorenz *et al.*[23]). This agrees well with the observed *a* lattice parameter for the CCS film grown on MgO, for which we used a higher oxygen pressure than for the films grown on *c*-sapphire, which show a (slightly) increased spacing of the $(\bar{6}03)$ planes. Due to the film thickness and the poor lattice match strain induced by the substrate material is unlikely the cause for this observation. A more probable cause is internal strain caused by a different oxygen stoichiometry or defects.

Another peculiarity of the thin films is the kink in the composition dependence of the lattice parameters at around 20 at. %, which is observed for both kinds of samples (see Fig. 5). Thus, it appears not to be related to the particular growth conditions applied by us.

The dependencies of the phonon mode energies for the thin films show a monotonous, smooth curve shape. It is mainly linear and shows a reasonably good match to the slopes obtained from the ceramic samples. These findings corroborate that the indium atoms are fully incorporated into the β-Ga_2O_3 lattice and the generally high crystalline quality of our films. For the ν_5 peak at $\omega_0 = 200\,cm^{-1}$, we observe a deviation between the samples on the two different substrates of about $2\,cm^{-1}$, while the other modes match very well (see Fig. 9). Further, the composition dependence of the spectral position of this particular peak exhibits a kink at the

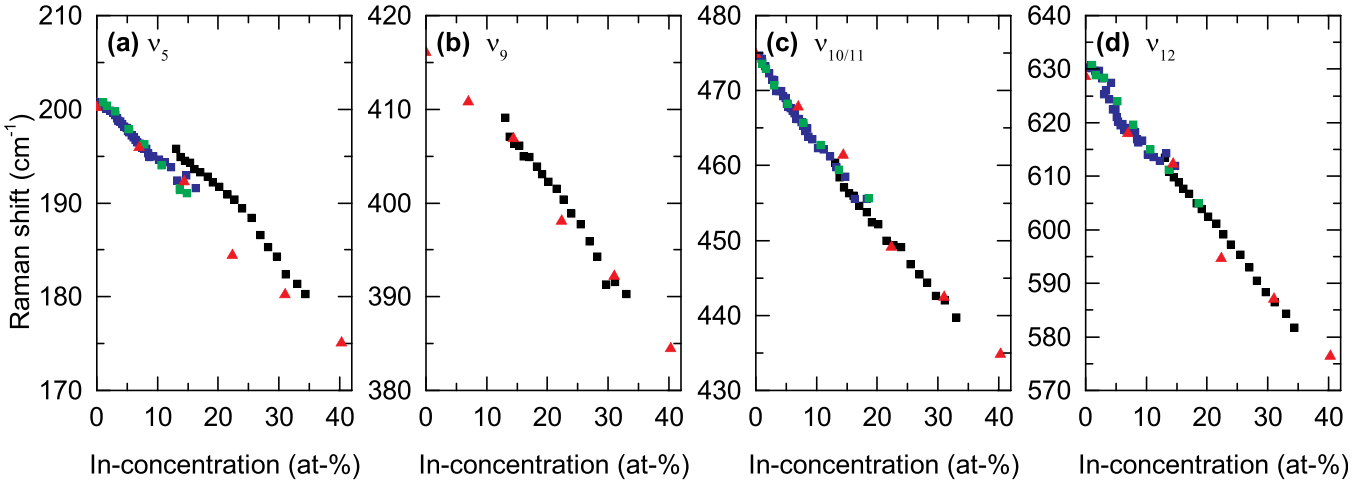

FIG. 9. Peak energies of four different phonon modes in dependence on the indium concentration in the sample. Data for the PLD targets are represented by red triangles, data for the films by squares, whereby data for the film grown on MgO are depicted in black, while data for the two films grown on *c*-sapphire are depicted in blue and green, respectively.

same composition for which we also observed a kink in the XRD data (see Fig. 5). This may be explained by a higher sensitivity of this phonon mode to the structural properties of the samples. The low energy vibrations up to about 300 cm^{-1} as the ν_5 mode are assigned to external vibrations, i.e., librational and translational movements of chains, while the higher energy modes are internal vibrations of metal oxide octahedra and tetrahedra.[7] Therefore, these higher energy modes are expected to be less sensitive to structural properties. However, this independence makes their investigation well suited for the determination of the composition based on the Raman spectra.

The rhombohedral $InGaO_3$ II phase was previously only reported for sample preparation under high pressure and equilibrium conditions. Oppositely, PLD applied here is a non-equilibrium process. Therefore, the formation of additional phases is possible also far away from the equilibrium conditions required for their incurrence. No Raman spectrum for this phase was reported before and it cannot be resolved individually in our samples as well. However, the peak at 260 cm^{-1} appears to be related to this phase and is therefore a good indication for its occurrence. Based on this, we were able to observe the critical indium concentrations above which this secondary phase is present in our films, which is ca. 20 at. % for the films on *c*-sapphire substrate and ca. 30 at. % for the films on MgO substrate, respectively. We note that, in Fig. 9, data for the β–$(In_xGa_{1-x})_2O_3$ phase are only shown for concentrations x before the formation of other phases. The occurrence of this phase probably also causes the much larger composition gradient of the samples grown on *c*-sapphire (see Fig. 1(d)), which is found at the lateral position, where the film reaches this critical concentration.

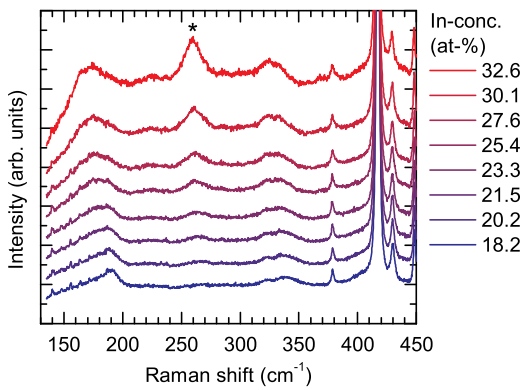

FIG. 10. Raman spectra of an $(In,Ga)_2O_3$ CCS thin film sample grown on *c*-sapphire. An additional mode (marked by an asterisk) develops around 260 cm^{-1} for $x > 0.2$.

V. CONCLUSIONS

We have determined the lattice parameters and spectral positions of eight Raman peaks for the $(In_xGa_{1-x})_2O_3$ ternary compound in dependence on the composition. The linear relations of the Raman modes on the indium concentration incorporated in the β-Ga_2O_3 host lattice were determined with high accuracy. Although the composition-dependent lattice parameters of our CCS thin films show a deviation from the ideal material, the phonon modes of the films exhibit essentially the same trend as the ceramic samples independent of the substrate and growth pressure used. Thus, the determination of the composition based on Raman spectroscopy is possible with a relative accuracy better than 10%. We further observed the occurrence of the rhombohedral $InGaO_3$ II phase in our samples and determined the indium concentrations above which it occurs to be about 20 at. % for *c*-sapphire substrates and 30 at. % for MgO substrates for the present growth conditions.

ACKNOWLEDGMENTS

C.K. was funded by the European Union and the Free State of Saxony. This work was supported within the framework of EFRE (SAB 100132251). We would like to thank Christian Dähne for carrying out part of the Raman measurements, Daniel Splith for programming a fitting script for the XRD data, Gabriele Ramm for the preparation of the PLD targets and ceramic samples, and Holger Hochmuth for thin film growth.

[1]D. D. Edwards, P. E. Folkins, and T. O. Mason, J. Am. Ceram. Soc. **80**, 253 (1997).
[2]G. Patzke and M. Binnewies, Solid State Sci. **2**, 689 (2000).
[3]S. J. Schneider, R. S. Roth, and J. L. Waring, J. Res. Nat. Bur. Stand. **65A**, 345 (1961).
[4]J. Macdonald, J. Gard, and F. Glasser, J. Inorg. Nucl. Chem. **29**, 661 (1967).
[5]C. Vigreux, L. Binet, D. Gourier, and B. Piriou, J. Solid State Chem. **157**, 94 (2001).
[6]R. Shannon and C. Prewitt, J. Inorg. Nucl. Chem. **30**, 1389 (1968).
[7]D. Dohy, G. Lucazeau, and A. Revcolevschi, J. Solid State Chem. **45**, 180 (1982).
[8]D. Machon, P. F. McMillan, B. Xu, and J. Dong, Phys. Rev. B **73**, 094125 (2006).
[9]B. Garcia-Domene, H. M. Ortiz, O. Gomis, J. A. Sans, F. J. Manjón, A. Muñoz, P. Rodríguez-Hernández, S. N. Achary, D. Errandonea, D. Martínez-García, A. H. Romero, A. Singhal, and A. K. Tyagi, J. Appl. Phys. **112**, 123511 (2012).
[10]C. Kranert, R. Schmidt-Grund, and M. Grundmann, Phys. Status Solidi RRL **8**, 554–559 (2014).
[11]H. von Wenckstern, Z. Zhang, F. Schmidt, J. Lenzner, H. Hochmuth, and M. Grundmann, CrystEngComm **15**, 10020 (2013).
[12]K. Matsuzaki, H. Hiramatsu, K. Nomura, H. Yanagi, T. Kamiya, M. Hirano, and H. Hosono, Thin Solid Films **496**, 37 (2006).
[13]T. Oshima, T. Okuno, and S. Fujita, Jpn. J. Appl. Phys., Part 1 **46**, 7217 (2007).
[14]L. Kong, J. Ma, C. Luan, W. Mi, and Y. Lv, Thin Solid Films **520**, 4270 (2012).
[15]S. Müller, H. von Wenckstern, D. Splith, F. Schmidt, and M. Grundmann, Phys. Status Solidi A **211**, 34 (2014).
[16]H. M. Rietveld, Acta Crystallogr. **22**, 151 (1967).
[17]D. Dohy and J. Gavarri, J. Solid State Chem. **49**, 107 (1983).
[18]Y. Kokubun, T. Abe, and S. Nakagomi, Phys. Status Solidi A **207**, 1741 (2010).
[19]Z. Mei, Y. Wang, X. Du, Z. Zeng, M. Ying, H. Zheng, J. Jia, Q. Xue, and Z. Zhang, J. Cryst. Growth **289**, 686 (2006).
[20]C. Y. Wang, L. Kirste, F. M. Morales, J. M. Mnuel, C. C. Rhlig, K. Khler, V. Cimalla, R. Garca, and O. Ambacher, J. Appl. Phys. **110**, 093712 (2011).
[21]E. J. Tarsa, J. H. English, and J. S. Speck, Appl. Phys. Lett. **62**, 2332 (1993).
[22]H. Sieber, S. Senz, and D. Hesse, Thin Solid Films **303**, 218 (1997).
[23]M. Lorenz, R. Böttcher, S. Friedländer, A. Pöppl, D. Spemann, and M. Grundmann, J. Mater. Chem. C **2**, 4947–4956 (2014).